

Differential Multiphoton Laser Scanning Microscopy

Jeffrey J. Field, Kraig E. Sheetz, Eric V. Chandler, Erich E. Hoover, Michael D. Young, Shi-you Ding,
Anne W. Sylvester, David Kleinfeld, and Jeff A. Squier

(Invited Paper)

Abstract—Multifocal multiphoton laser scanning microscopy (mfMPLSM) in the biological and medical sciences has the potential to become a ubiquitous tool for obtaining high-resolution images at video rates. While current implementations of mfMPLSM achieve very high frame rates, they are limited in their applicability to essentially those biological samples that exhibit little or no scattering. In this paper, we report on a method for mfMPLSM in which whole-field detection with a single detector, rather than detection with a matrix of detectors, such as a charge-coupled device (CCD) camera, is implemented. This advance makes mfMPLSM fully compatible for use in imaging through scattering media. Further, we demonstrate that this method makes it possible to simultaneously obtain multiple images and view differences in excitation parameters in a single scan of the specimen.

Index Terms—Fluorescence microscopy, nonlinear microscopy, nonlinear optics, second-harmonic generation (SHG), two-photon microscopy, ultrafast optics.

I. INTRODUCTION

OWING to its numerous advantages over confocal microscopy, multiphoton laser scanning microscopy (MPLSM) has become a vital tool for obtaining high-resolution images of biological tissues in a relatively noninvasive manner. Due to the nature of the nonlinear excitation process, MPLSM has proven especially useful for imaging deep into highly scattering biological tissues [1], [2]. Furthermore, MPLSM can be performed with several contrast mechanisms, including nonlinear absorption [3] and nonlinear fluorescence [1], harmonic

generation [4]–[7], and nonlinear scattering processes [8], [9]. Each of these mechanisms allows one to gain insight into the structure and function of the sample under study via the localization of nonlinear response.

Since it was first introduced in 1998 [10], [11], multifocal MPLSM (mfMPLSM) has been a useful extension of MPLSM for high-speed image acquisition. By separating a single excitation focus into several foci, the area each focus must scan may be decreased, thereby increasing the speed with which successive frames may be acquired. Unfortunately, multifocal systems suffer from several disadvantages often associated with wide-field microscopes, thereby reducing or eliminating the advantages gained by MPLSM. The largest restriction in mfMPLSM setups is the need to use imaging detectors to accurately map the nonlinear signal generated by each focus [12], resulting in a reduction in resolution in scattering samples, and negating other advantages of MPLSM for highly scattering media.

In this paper, we report on a system for imaging with multiple foci that does not require an imaging detector. Instead, a single-element detector, e.g., a photomultiplier tube (PMT), is used to collect the nonlinear signal generated by each focus inside the sample. The signal measured by the PMT is electronically demultiplexed to attribute photons to the appropriate focus, or voxel. This allows one to collect images from multiple foci while maintaining the whole-field detection typical of MPLSM, making it possible to image through highly scattering media. Further, we show that the nature of this optical system leads to a new type of microscopy, dubbed *differential MPLSM* (dMPLSM), that makes it possible to simultaneously obtain multiple images and view differences in excitation parameters in a single shot. In the dMPLSM setup described here, the beams that generate each foci are spatially separated, making it possible to control the modality of each focus individually. The result is a set of simultaneous images that highlight the differences resulting from varied excitation parameters.

The dMPLSM system that we describe contains a number of advancements, which are of relevance for imaging in dynamic biological systems. These include the following.

- 1) Whole-field detection of multiple modalities with multiple foci. This is especially useful for imaging deep into living brain tissue that is tagged with multiple fluorophores [13], or where multiple nonlinear modalities, such as harmonic generation and nonlinear fluorescence, are of interest [14].
- 2) The use of an electronic z -axis control with a simple piezoelectric controller.

Manuscript received June 10, 2010; revised September 9, 2010; accepted September 9, 2010. This work was supported by the National Institute for Biomedical Imaging and Bioengineering under Grant BRP EB-003832 and by the National Science Foundation (Renewable Energy Materials Research Science and Engineering Center). The work of A. W. Sylvester was supported by Division of Biological Instrumentation under Grant 0501862.

J. J. Field, E. V. Chandler, E. E. Hoover, M. D. Young, and J. A. Squier are with the Center for Microintegrated Optics for Advanced Bioimaging and Control, Department of Physics, Colorado School of Mines, Golden, CO 80401 USA (e-mail: jjfield@gmail.com; echandle@mines.edu; ehooover@mines.edu; miyoung@mines.edu; jsquier@mines.edu).

K. E. Sheetz is with the Department of Physics and Nuclear Engineering, U.S. Military Academy, West Point, NY 10996 USA (e-mail: kraigsheetz@gmail.com).

S. Ding is with National Renewable Energy Laboratory, Golden, CO 80401 USA (e-mail: Shi.you.Ding@nrel.gov).

A. W. Sylvester is with the Department of Molecular Biology, University of Wyoming, Laramie, WY 82071 USA (e-mail: annesyl@uwyo.edu).

D. Kleinfeld is with the Department of Physics, University of California at San Diego, La Jolla, CA 92093 USA (e-mail: dk@physics.ucsd.edu).

Color versions of one or more of the figures in this paper are available online at <http://ieeexplore.ieee.org>.

Digital Object Identifier 10.1109/JSTQE.2010.2077622

- 3) Simultaneous excitation at multiple wavelengths.
- 4) Simultaneous acquisition of multiple frames at video rates.

Each of these imaging modalities is highly beneficial for numerous assays.

II. MULTIFOCAL MULTIPHOTON MICROSCOPY (mfMPLSM)

mfMPLSM has been implemented in a number of configurations for biological imaging applications. In all previous cases, a single femtosecond laser pulse is split into multiple pulses, each of which is relayed to the sample plane in the microscope. By careful design of the image relay optics, each focus is spatially, and in some cases temporally, offset from the others to prevent interference and preserve spatial resolution. Thus, instead of a single focus in the specimen plane of the microscope, an array of foci is generated, each of which has sufficient energy to generate nonlinear contrast. While the methods used to generate multiple foci in a microscope can vary, the use of mfMPLSM is motivated by two shortcomings of MPLSM systems.

First, a typical MPLSM setup is extremely inefficient when used with optically thin preparations so that the loss of incident power as a result of scattering can be ignored. The femtosecond laser source is driven by an optical pump beam and operates at somewhere around 20%–30% efficiency. In the case of most commercial titanium-doped sapphire ($\text{Ti:Al}_2\text{O}_3$) oscillators, for example, 2 W of average power in the femtosecond beam requires the cavity to be pumped with green laser light at ~ 10 W. The overall efficiency is further degraded by the fact that 2 W of power is far too high for biological preparations. Several published accounts have indicated that the peak intensity that can be tolerated by most biological tissues is roughly 200 GW/cm^2 for pulses 200 fs in duration [15], [16]; therefore, only a small portion of the available pulse energy may be used for imaging. For example, with laser pulses 200 fs in duration arriving at 80 MHz, 2 W of average power will result in a peak power of $\sim 80 \text{ kW}$. If the objective used for imaging focuses the laser to $1 \mu\text{m}^2$ in the specimen, an average power of just $\sim 50 \text{ mW}$ is needed to generate 200 GW/cm^2 in the sample plane (cf., Appendix), implying that only about 2.5% of the oscillator power is used to image. If a throughput efficiency of 50% is assumed for the relay optics from the laser cavity to sample plane, then just 5% of the laser power available at the focal plane may be used. Clearly, this is a waste of excitation photons.

mfMPLSM uses excess laser power to split a single focus into multiple foci, thereby placing the maximum average power into N beams. If, for example, one images with 16 foci, then the average power incident on the sample may be increased 16-fold, resulting in 770 mW of average power in the sample plane. As long as this amount of average power does not adversely affect the specimen by heating in the sample plane, excitation photons may be used much more efficiently, $\sim 80\%$ of the 1-W throughput in this case instead of $\sim 5\%$.

A complementary reason for switching to an mfMPLSM setup from a standard MPLSM setup is to improve image-acquisition speeds. Biological samples are inherently 4-D, which requires that a 3-D data stack be obtained with enough temporal resolution to resolve dynamic processes occurring within the

sample. This is the ultimate goal of mfMPLSM in the biological sciences—to study the 4-D behavior of a specimen with high spatial and temporal resolution, all without damaging the sample.

All laser scanning microscopes are limited in their image-acquisition time by the read time of the detector, the scan rate of the beam-rastering mechanisms, and the photon yield of the nonlinearity used to generate image contrast. To acquire a 3-D image in a typical MPLSM apparatus, the focal volume must be rastered across the sample in a 2-D plane, and then either the sample or the excitation objective is translated and another 2-D image is acquired. This process is continued until the desired volume within the sample has been imaged. In a common imaging scheme with galvanometric scan mirrors, frame rates of $\sim 10 \text{ Hz}$ are typically achieved for 200×200 pixel images with 0.5 ms line speeds. As line speeds in the axial direction are typically an order of magnitude slower, it is difficult to resolve dynamic processes that span 3-D in living tissues. Many examples of solutions to this fundamental limit in acquisition speed have been proposed, such as nonlinear holographic microscopy, and nonlinear wide-field microscopy [17]. While these methods improve the 3-D acquisition rate by either imaging a 3-D field of view (FOV) or by negating the need for 2-D scanning in the lateral plane, they suffer from some disadvantages that are circumnavigated by MPLSM with single-point excitation.

Until recently, all mfMPLSM setups reported on have generated a laterally dispersed 2-D array in the focal plane of a multiphoton microscope. While this is a very effective means of greatly reducing the scan time required in the lateral plane, and thus improving total volume image-acquisition times, these setups are still limited by the speed at which the specimen or excitation objective may be translated to achieve axial scanning. Recently, we reported on several variations of a simple optical multiplexing scheme using a single beam splitter to generate two foci for mfMPLSM [14], [18]–[20]. However, instead of spatially orienting our foci in the lateral plane, we make the two foci collinear and offset them axially to achieve volumetric imaging. The unique photon-counting and electronic demultiplexing used to attribute signal photons to their proper point of origin in the sample make it possible to simultaneously collect images from multiple planes. While this system was developed with the intent of performing mfMPLSM in volumetric imaging modality by generalizing to N foci, the two-foci system has the distinct advantage that the various excitation parameters of each focus, such as polarization and spectral content, may be varied independently to enable dMPLSM and many new experimental assays.

The greatest advantage of the dMPLSM system outlined in this paper is its ability to characterize these differences in a single scan of the beam rastering mechanism. While it is possible to, for example, image with varying polarization states by taking one image, changing the polarization state and imaging again, this is an impractical method in dynamic specimens. By allowing for these differences to be visualized simultaneously, dMPLSM makes it possible to observe such differences *in vivo*, or as a sample undergoes a phase or conformational change.

A. Antecedents to mfMPLSM

One of the first methods demonstrated for improving the 2-D image-acquisition time in MPLSM was line scanning [21], in contrast with point scanning, in which the excitation source is focused with cylindrical optics to create a line-focus within the sample, negating the need for scanning in one lateral direction. This allows one to scan above video rates in the sample with typical scanning mechanisms. Although this greatly reduces the 2-D image-acquisition time, the axial resolution suffers due to the fact that fewer high-spatial-frequency components are included in the cone of focused light [11], [22]. Therefore, while it is possible to attain diffraction-limited resolution in the laterally focused direction, the axial resolution is worse than could be obtained with spherical focusing optics.

One means to restore the inherent optical sectioning capability of MPLSM is to simultaneously focus the excitation source in both space and time [23]. This is accomplished by spatially dispersing the spectral content of the beam prior to the focusing objective such that the duration of the pulse is shortest only in the spatial focus of the laser. Since the intensity of the focused beam strongly depends on the pulse duration, appreciable nonlinear absorption or scattering occurs only where the pulse is short, reducing the axial extent of the nonlinear interaction. This method has been demonstrated to result in axial resolutions of 1.5 μm , with image-acquisition time of approximately 100 ms [24]. However, the axial resolution is gained at the expense of lateral resolution, since the excitation objective cannot be overfilled in one lateral direction at its back aperture, and the images obtained are essentially wide-field MPLSM images.

Wide-field MPLSM is another method for solving the image-acquisition time problem by negating the need for scanning in the lateral dimension. By underfilling the excitation objective in both lateral directions to obtain a large focus within the specimen plane, Fittinghoff *et al.* demonstrated wide-field MPLSM [17]. By negating the need for scanning in the lateral dimensions, image acquisition at video rates (30 Hz) were attained.

Finally, MPLSM by multipoint excitation was proposed and demonstrated by two separate groups in 1998 [10], [22]. Since then, mfMPLSM has developed steadily and is becoming a standard tool for high-speed image acquisition.

B. mfMPLSM: The Current State of the Art

As stated earlier, mfMPLSM is most often implemented to reduce scan times and improve image-acquisition speeds. By scanning an array of foci in the specimen, the area that an individual focus must scan in order to obtain an image of the same FOV with a single focus is drastically reduced. As a consequence, the scanning mechanism, such as galvanometric scan mirrors, must map out only a fraction of the area that they do with a single focus. In practice, the area is reduced from the whole FOV to FOV/N , where N is the number of foci, and the time required to image the same FOV is thereby decreased.

In the first demonstration of mfMPLSM by Bewersdorf *et al.* [10], [15], a spinning disk containing an array of microlenses was used to rapidly scan the specimen at 225 Hz. While Bewersdorf *et al.* were able to scan the FOV at this rate,

they were limited by the readout time of the charge-coupled device (CCD) camera used to image the nonlinear signal to 32 Hz for a 480×640 pixel image, and 67 Hz for a 384×384 pixel image. Both of these acquisition rates are greater than the video rate of 30 Hz, and consequently a real-time image could be viewed either on the CCD, or in the eyepiece of their multiphoton microscope [10]. Soon after the demonstration, another use of microlens arrays was reported in which real-time image acquisition under two-photon-excited fluorescence (TPEF) was observed. This strategy involved using a stationary microlens array instead of an array on a rotating disc, and rapidly scanning the 2-D array of foci generated by the lens array with a pair of galvanometric scan mirrors [11]. Again, a CCD camera was used and made it possible to view an image of the specimen under study in real time.

When adjacent laser pulses arrive at the same time, interference enhances off-axis components of the electric field and degrades the spatial resolution of many mfMPLSM setups [11]. Since MPLSM is performed with ~ 100 -fs-duration pulses, a small temporal delay between pulses that overlap spatially mitigates this effect and permits diffraction-limited mfMPLSM to be performed. In one such implementation, picosecond delays were generated between adjacent pulses in the scanning disc microlens array method by addition of small delay plates on each lens of the disc [25]. Another solution generated delays between pulses by the use of cascaded beam splitters, thereby using the optical path length difference of each pulse to generate delay [26]–[28]. Both methods were successful in achieving diffraction-limited mfMPLSM at or beyond video rates. An additional advantage of the beam splitter setup, however, is the ability to easily adjust the spacing between adjacent foci within the sample. In principle, it is possible to space the temporally delayed pulses so close to one another that scanning can become unnecessary, allowing for wide-field detection by multipoint excitation [28].

Another solution for optical multiplexing mfMPLSM was to use diffractive optical elements (DOE) to generate multiple foci in the sample plane [29], [30]. This method has the tremendous advantage of adjustable focal densities by simply modifying the period of the diffractive mask, which can be accomplished electronically with various DOEs. On the down side, this method produces unequal intensities in the array of foci that result from the variation in the spatial-intensity profile of the incident excitation beam. Thus, differences in signal intensity must be numerically or electronically corrected to obtain a homogenous response in the sample plane.

Despite the advantages of these mfMPLSM setups for image-acquisition speed, an inherent disadvantage is the need to optically image the nonlinear signal to a multipoint detector, such as a CCD camera for spatial registration.

C. Drawbacks to mfMPLSM in Biological Tissues

One of the main advantages of MPLSM over conventional linear microscopy in the biological sciences is its ability to produce high-resolution images through highly scattering media [1], [2], [12]. While it is often sufficient to image *in vitro* samples

by histologically constructing a 3-D dataset of the specimen, for many applications, this method is unacceptable. An example of such a case is *in vivo* imaging of blood-flow restoration following a targeted insult to the vasculature of cortical tissue in live rodents [31]. By imaging deep within the tissue, one has the ability to study how blood flow is redirected during stroke or aneurism.

Currently, imaging depths are limited to approximately 600 μm with conventional femtosecond oscillator sources (i.e., Ti:Al₂O₃ oscillators centered at 800–950 nm), although depths of up to 1 mm have been achieved with amplified systems [32], and by use of sources with wavelengths further into the near-infrared spectrum [33].

Several aspects of scattering limit the imaging depth in biological samples. First, the only photons from the excitation source that are able to contribute to nonlinear excitation are the so-called ballistic photons [2], that is, the photons that undergo no scattering between the objective lens and the geometric focus of the laser beam. Thus, any excitation light that is scattered reduces the amount of nonlinear signal generated by reducing the intensity of the excitation source at focus. The decay in power reaching the focus decreases exponentially with penetration depth in a scattering sample [2]. Given the nonlinear dependence of the generated contrast signal on the intensity of the excitation source, this can cause a significant reduction in the number of signal photons generated deep within scattering media.

Furthermore, the signal photons are subject to scattering as well. Due to conservation of energy in both two-photon excitation and harmonic generation, the wavelength of signal photons is always shorter than that of the excitation light in MPLSM. Since the mean scattering length, that is the average length a photon travels in a medium before it is scattered, is reduced with decreasing wavelength, signal photons in highly scattering tissues are subject to significant amounts of scattering that degrades the measured signal further.

In all of the mfMPLSM implementations discussed in the previous section, imaging detection is required to map the origin of a signal photon to the region of origin, as small as 0.5 fL (see Appendix) within the sample plane. This is done by simple relaying optics to image the specimen to a 2-D detector, such as a CCD camera [10], [15]. While this method is very straightforward and has the advantage that very fast frame rates can be achieved, the ability to attain high-spatial-resolution images deep within scattering tissues is greatly reduced [34]–[36]. In highly scattering media, signal photons that are scattered appear to originate from a position other than that of the focal volume, and thus appear out of focus [2], [12]. This is not, however, an issue in weakly scattering tissue, or at shallow depths within strongly scattering specimens. Several published reports have demonstrated that as one images deeply into strongly scattering media, the resulting image begins to blur [34]–[36]. While there are methods such as confocal detection arrays to reduce this effect, it is still an undesirable method for imaging deep in biological tissues.

One solution to the spatial mapping problem in scattering media is to use multiple-anode PMT detectors with the number of

anodes matched to the number of foci [36]. By descanning the nonlinear signal, each focus is essentially treated like a single-focus MPLSM system would be, each anode integrating signal from a large FOV. While this study demonstrated that blurring due to scattered photons is indeed greatly reduced, this method is still limited by image blurring due to crosstalk between anodes from scattered photons. While this can be effectively removed to achieve deep imaging within brain tissue, it requires postprocessing deconvolution techniques [36].

By approaching the problem of mfMPLSM in a different manner, we have demonstrated that it is possible to collect nonlinear signal photons from multiple foci by electronically demultiplexing the signal from single-element detectors, such as a single-element PMT or avalanche photodiode, eliminating the need to spatially register each signal photon by image relay optics. Using this method, we have shown for the first time that it is possible not only to achieve mfMPLSM with an MPLSM detection scheme, but that postprocessing is no more necessary in our mfMPLSM system than in a typical MPLSM system. Furthermore, by negating the need for imaging optics or descanning, we are able to simultaneously measure multiple modalities [14], [20]. Although multimodal mfMPLSM has been performed by imaging second-harmonic generation (SHG) in the transmissive direction and fluorescence in the epi-direction [37], no other method of mfMPLSM has achieved MPLSM detection in multimodal experiments. Given the shorter wavelength of harmonic generation, the signal photons in such an experiment are subject to more scattering, and therefore, blurring, than the fluorescence photons. Thus, this system is capable of not only collecting images from multiple foci in a single shot, but also from multiple modalities while maintaining the whole-field detection inherent in MPLSM.

III. DIFFERENTIAL MULTIPHOTON LASER SCANNING MICROSCOPY (DMPLSM): A NEW APPROACH TO MFMPPLSM

We view the problem of data acquisition in MPLSM from a different perspective, and consequently have developed a mfMPLSM scheme that not only improves imaging rates, but also opens the door for direct comparisons of varying excitation parameters to be visualized in a single shot. Instead of approaching the problem of mfMPLSM by generating an array of foci in the lateral focal plane, we generate multiple foci in the axial plane. By then extending the delay between adjacent pulses to nanosecond instead of picosecond durations, and employing photon-counting detection, we are able to electronically demultiplex the nonlinear contrast signal from the specimen to obtain multiple images simultaneously, the basis of DMPLSM.

A. Optical Multiplexing

There are several methods for generating multiple foci in an mfMPLSM system. In our implementation, we generate two foci that are spatially collinear, but we temporally delay one pulse by one-half of the period of the oscillator. This is accomplished by constructing an interferometer-like setup with a polarizing beam splitter (PBS) and two retroreflecting mirrors [see Fig. 1(a)]. By careful alignment of these elements, it is possible to achieve

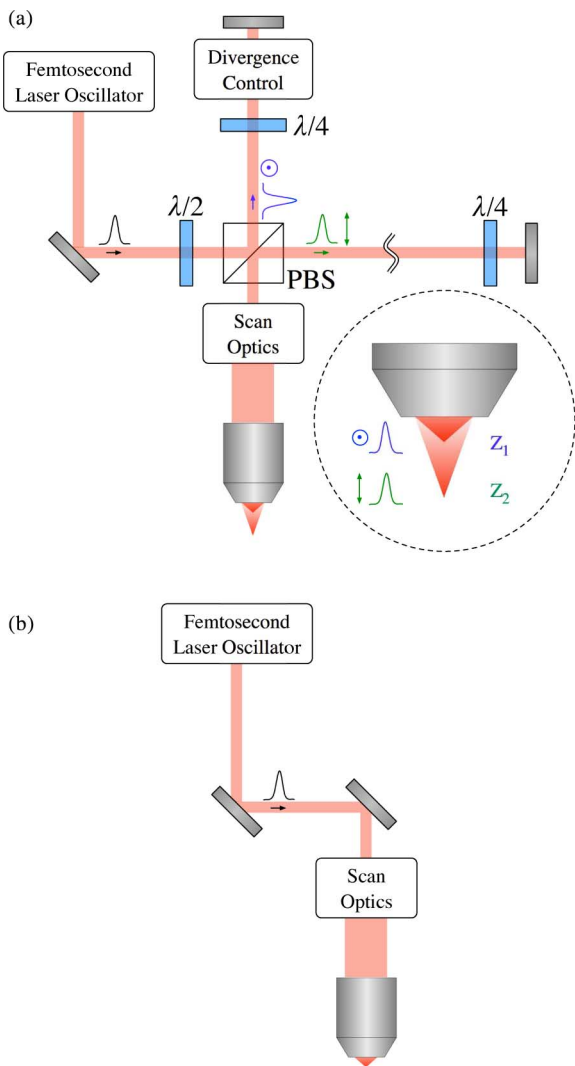


Fig. 1. Comparison of (a) optical demultiplexing used for the dMPLSM system and (b) traditional MPLSM imaging system. Generating two collinear beams to achieve two orthogonally polarized foci in the sample plane is done with straightforward optical components, and optical delay by path length modification is used to achieve interlacing of pulse trains.

collinear laser pulse trains. For comparison, the corresponding diagram for a typical single-point MPLSM system is represented in Fig. 1(b). In both diagrams in Fig. 1, the scan optics include a beam rastering mechanism, and can contain beam expanding telescopes or other optics for proper telecentric scanning.

Since a single pulse is split into two using a PBS, a $\lambda/4$ waveplate is inserted into each beam path such that the polarization state of the beam is rotated by 90° upon double passing the waveplate. This ensures that each pulse will be transmitted through the PBS toward that scan optics. By using polarization state to split our single beam into two, the pulse train in the scan optics consists of an interlaced train of pulses from each arm of the interferometer, every pulse being orthogonally polarized with respect to those adjacent to it. This pulse train is focused into a specimen as though it were a single-focus MPLSM system [see Fig. 1(a)].

To date, we have used two sources for this method, one an extended cavity $\text{Ti:Al}_2\text{O}_3$ oscillator with a repetition rate of 21.7 MHz [14], [18], and the other a $\text{Yb:KGd(WO}_4)_2$ oscillator with a repetition rate of 56 MHz [20]. One pulse from the beam splitter is delayed with respect to the other by either 23 ns or 9 ns, depending on the excitation source. Due to the additional path length experienced by one of the two beam paths, which corresponds to one full cavity length of the oscillator, each beam focuses to a slightly different depth within the specimen. This is due to the additional divergence experienced by the beam with a longer optical path length. While this can be overcome by the addition of a simple telescope to the longer arm, we have found it more useful to insert user-defined divergence control into one arm of the interferometer, as shown in Fig. 1(a). This can be done in any number of ways, including passive telescopes [20], deformable mirrors [14], [18], and image relaying with objective lenses [38]. This allows for programmable control of the axial spacing between the two foci in the specimen plane.

Altogether, the foci in the specimen are separated in time by tens of nanoseconds, have orthogonal polarization states, and can be separated axially by a user-defined amount. The temporal separation and orthogonal polarization states make it possible to spatially overlap the foci within the sample without interference. Since the beams are collinear, the same 2-D plane is scanned in the specimen by each focus. Furthermore, we are able to modify other properties of each pulse separately. As we will demonstrate later, this can be greatly advantageous for many assays in biological MPLSM.

B. Electronic Demultiplexing

In order to avoid the limitations of most mfMPLSM setups due to imaging detection, we take advantage of the nanosecond separations between pulses to electronically demultiplex the nonlinear signal measured by a single-element detector. Detailed electronic layouts and demultiplexing procedures are discussed at length in [20]. In brief, the laser pulse train is incident on a dichroic mirror that transmits the excitation light, and reflects the nonlinear signal toward the PMT in the epi-direction [see Fig. 2(a)]. At a point before the scan mirrors, a glass slide is inserted into the pulse train to reflect a small portion of the laser intensity to a photodiode detector. The analog signal from the photodiode is denoted the laser clock (LC) and serves as the phase reference for demultiplexing. Since we may safely assume that at most we generate one signal photon per laser pulse [39], there is no need to consider multiple signal photons for a clock pulse. This allows us to use the interlaced pulse train as a clock signal for an electronic demultiplexer.

Both the LC and PMT signals are thresholded, and converted to TTL logic pulses [see Fig. 2(b)], which are then fed into a field-programmable gate array (FPGA). The FPGA is programmed to contain two counters, one for each focus. As each signal photon occurs under the envelope of a LC pulse, it is possible to rapidly switch between counters to attribute signal photons from each focus to their appropriate position in the sample. For every pixel in the image, the counters are set to zero, and signal photons are incrementally counted for each focus in

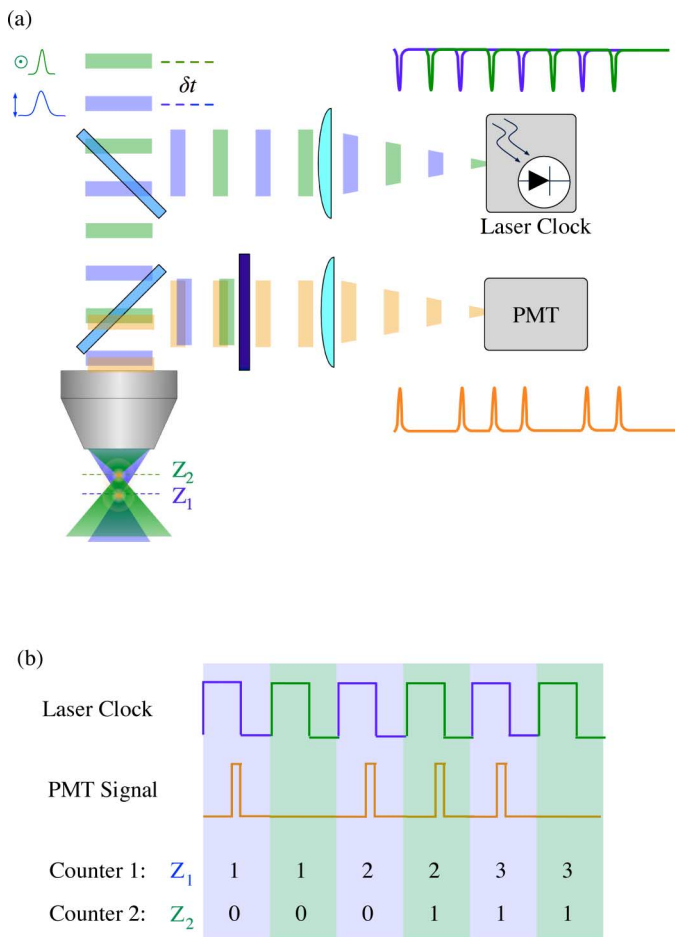


Fig. 2. Explicit schematic of (a) optical multiplexing and (b) electronic demultiplexing used in the dual-focus dMPLSM system.

the specimen. Once the dwell time is reached, both counters are reset to zero and the scan mirrors move to the next position in the sample. During scanning, the count for each pixel of each image is stored in the memory of the FPGA, and is downloaded to a computer after each frame is scanned. By electronically demultiplexing the nonlinear signal out of a single-element PMT, we are able to simultaneously acquire two images from a single scan. This is the heart of dMPLSM, as it allows us to vary the excitation parameters of each foci to visualize the difference in specimen response simultaneously. This detection scheme is easily scalable to multimodal detection by additional detection pathways in the microscope and additional FPGAs for each detector.

Beyond electronic demultiplexing, photon counting has additional advantages. It yields an improved SNR compared with analog detection, as noise associated with single-photon variability in the output of the PMT, i.e., pulse-height variability, is negated. We have obtained noise levels on the order of 10–50 counts in a 1-s image. For a 512×512 pixel image, this amount of noise per pixel is nearly negligible, resulting in a very good SNR. Second, photon counting allows for quantitative imaging assays with mfMPLSM to be performed. In particular, the num-

ber of signal photons measured at one focus may be compared to the number measured with the other.

IV. RESULTS

We consider four proof-of-principle demonstrations of our dMPLSM setup.

A. Depth dMPLSM

We are able to simultaneously extract two planes, while simultaneous imaging of up to six planes has been demonstrated [19], [40]. This allows for volumetric imaging in the whole-field MPLSM detection scheme by obtaining data from a 3-D volume in a single scan. This is demonstrated for two foci in Fig. 3, where two planes in a transgenic maize plant expressing enhanced yellow fluorescent protein were acquired simultaneously. Due to the relatively small two-photon action cross section over the bandwidth of the Ti:Al₂O₃ laser oscillator used to acquire the images shown in Fig. 3 (approximately 2.5–8.0 Göppert–Mayers over the range 790–825 nm; [41]), the TPEF intensity is largely due to endogenous fluorescence from the maize plant. Not only does depth dMPLSM allow for the sample to be viewed in multiple axial planes simultaneously, but it also makes it possible to perform rudimentary particle-tracking measurements in 3-D, both of which are useful for many biological assays.

In order to obtain depth dMPLSM images, the two foci must be offset axially with some method of divergence control. We accomplish this with a setup based on relaying an image of the focus from an external objective to the excitation objective [38]. By placing an objective lens in the short arm of the DMM setup and image relaying the back aperture of that lens to the back aperture of the excitation objective, a piezoelectric mirror in the short arm of the dMPLSM setup can be used to control the axial position of the focal plane of the short arm in the specimen (see Fig. 4.) This allows us to quickly control the spacing between the two foci, as the response time of the piezoelectric actuators is on the order of milliseconds.

To test the axial scanning capability of this system, we measured the third-harmonic-generation (THG) signal from two cover slips separated by 90 μm of wax film. The axial response for THG from cover slips has been well characterized [6], [7]; therefore, we may use this sample to perform a characterization of the axial scanning capabilities of this system. The THG response shows us not only how far the system can scan, but allows us to see if the excitation point spread function (PSF) degrades as the axial position is changed. Fig. 5 shows the results of this axial scan over a range of 120 μm . The full-width at half-maximum (FWHM) of the axial THG response at the second interface was fit with a Gaussian envelope and found to be approximately 7.5 μm , a value in good agreement with the theoretical value of 6.9 μm , calculated following the mathematical formalism outlined in [42] for an excitation wavelength of 1039 nm, numerical aperture of 0.65, and assuming nBK7 as the glass type. Note also that the first peak in the axial THG response is broader and asymmetric, a result of spherical aberration in the focusing system [6].

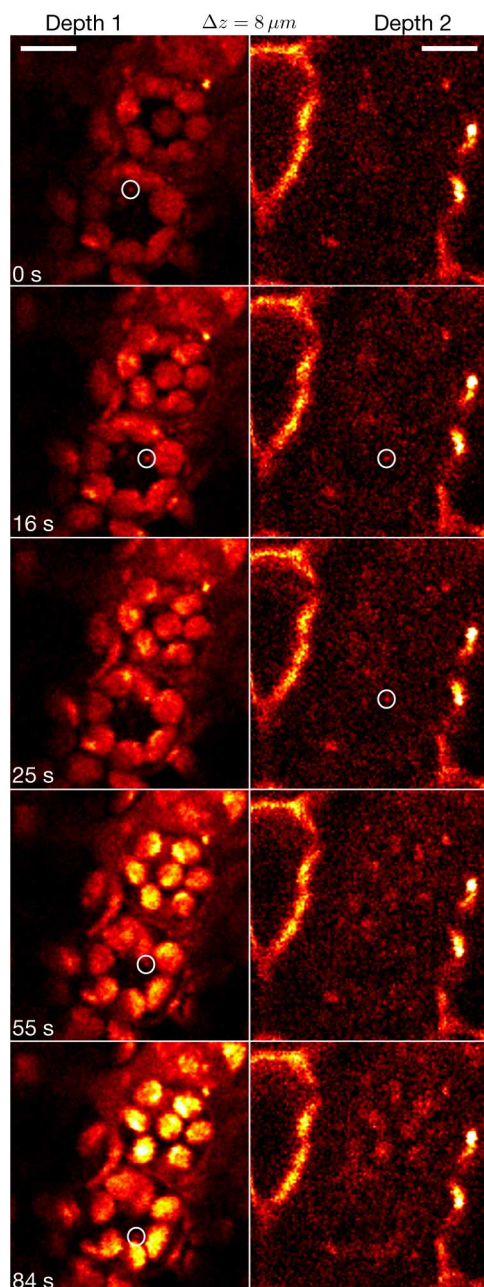


Fig. 3. Simultaneous images separated by $8 \mu\text{m}$ axially in the epidermis of a maize leaf transgenically modified to express enhanced yellow fluorescent protein. Circles indicate the location of a feature within the specimen that moves over time, which can be seen in both depths simultaneously. Scale bar is $10 \mu\text{m}$.

We compared 3-D datasets acquired with specimen scanning and by scanning the piezoelectric mirror (see Fig. 6). There is very good agreement between the two datasets, over a total axial range of $42 \mu\text{m}$ in this image set, which indicates that we are capable of scanning a large area axially in scattering media. Moreover, the resolution of the dataset is nearly identical for both methods when imaging deeper in the tissue, confirming that one can maintain tight focusing with this scheme. One important point to note when comparing the image series in Fig. 6 is that the piezoelectric scanning and specimen scanning do not necessarily scan the same axial planes in the specimen.

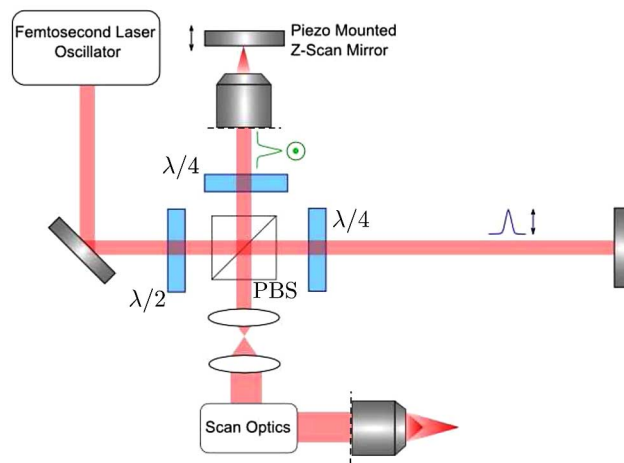


Fig. 4. Schematic of system used for depth scanning with a piezoelectric actuated mirror. The two lenses image relay the back aperture of the first objective to the back aperture of the excitation objective (dashed lines).

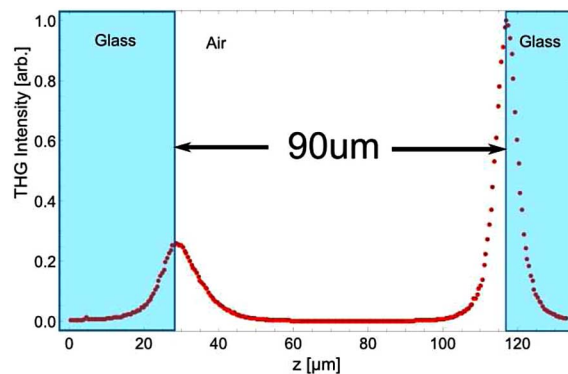


Fig. 5. THG response measured from the glass/air interfaces of two cover slips separated by $90 \mu\text{m}$. The axial THG response demonstrates that the excitation PSF is not significantly degraded over the $120\text{-}\mu\text{m}$ scan range.

We can correlate the maximum and minimum depths in the specimen, but the axial spacing in the piezoelectric scanning dataset differs from those in the specimen-scanning set.

Finally, this method could easily be extended to achieve arbitrary scan planes in the specimen by coupling the scan mirrors for the lateral plane with the piezoelectric mirror in the appropriate manner to achieve the desired pattern. This would allow one to rotate the 2-D scan plane in a specimen by simply programming the scanning electronics for all three degrees of freedom, a capability that could be greatly advantageous in a myriad of biological MPLSM applications.

B. Polarization *dMPLSM*

Many processes in nonlinear optics are highly dependent upon the polarization state of the excitation source. For harmonic generation, this is a result of the phase-matching conditions necessary to give an appreciable signal. Phase matching in MPLSM can be a very valuable tool for determining orientation of structures within biological specimens without the need for an exogenous fluorophore. In particular, SHG from fibrous

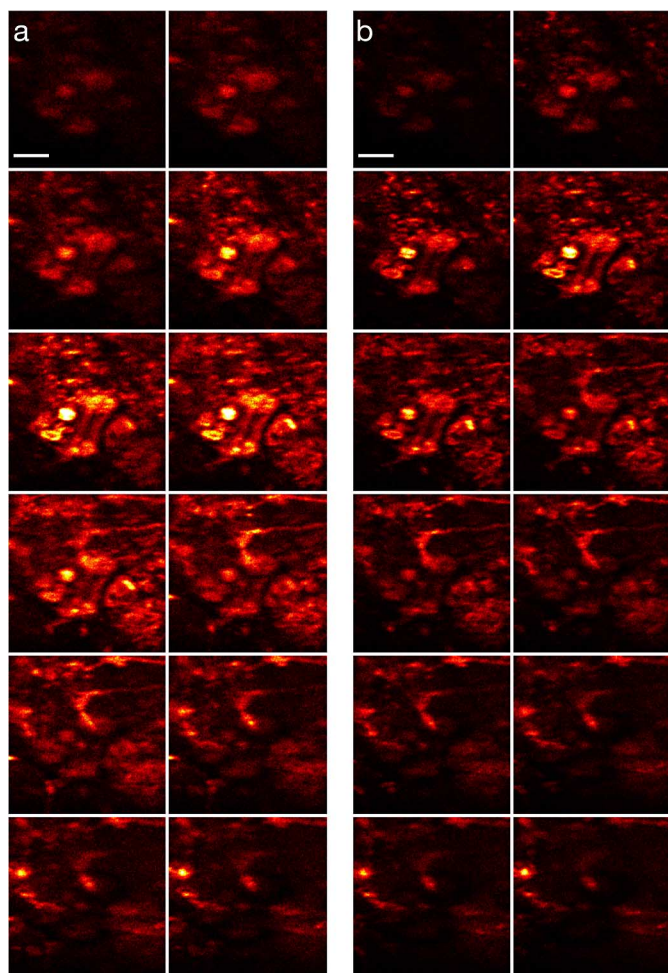


Fig. 6. Direct comparison of axial scanning with (a) piezoelectric mirror and (b) specimen stage. Total axial scan range is $42\ \mu\text{m}$ in transgenic maize epidermis expressing enhanced yellow fluorescent protein. Intensity maps represent fluorescent intensity. Notice that the spatial resolution with the piezoelectric scanning mechanism is as good as the specimen scanning results, indicating that tight focusing is maintained throughout the scan range. Scale bars are $10\ \mu\text{m}$.

structures such as rat tail tendon [43] and crystalline cellulose strands [20], [44], [45] have been shown to not only have a strong dependence upon the orientation of excitation polarization, but also have been used to show that the harmonic signal generated in the forward- and backward-propagating directions are dependent on factors, such as sample density, mean scattering length, and structural size and orientation. This allows one to not only visualize intensity maps of the specimen to gain insight into the structure of a sample, but also to understand phase-matching conditions within the structure by collecting images with varying polarization states.

One example of such a polarization-dependent sample is simple corn starch [14]. Amylopectin chains in corn starch grains, the molecule responsible for SHG, are arranged azimuthally along the grain. Since only those molecules that are parallel to the input polarization state satisfy the phase-matching conditions necessary to generate SHG, one does not see the entire grain in an SHG image of corn starch. Moreover, the central

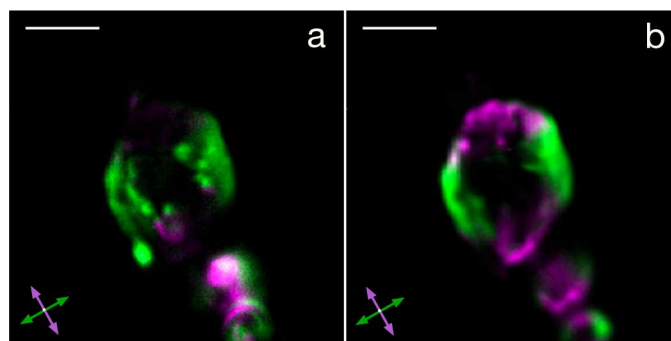


Fig. 7. Polarization dMPLSM in SHG for both the (a) transmission and (b) epi-directions. Purple and green arrows indicate the orientation of the polarization state corresponding to the region of the sample that is visible in the image. Regions in white appear where the response from each polarization overlaps with the same intensity. Note that each figure is composed of two images taken at orthogonal polarizations. All four images comprising this figure were taken with a single scan of the galvometric mirrors, using a $\text{Ti:Al}_2\text{O}_3$ oscillator focused by a $0.75\ \text{NA}/40\times$ objective (Olympus, UPlanFL). Scale bars are $10\ \mu\text{m}$.

portion of the grain is centrosymmetric, meaning that SHG cannot occur from this region regardless of the polarization state of the excitation source. Consequently, when images are taken with orthogonal linearly polarized beams, two different sets of lobes of each starch grain are activated. This is demonstrated in Fig. 7, in which the SHG response of corn starch grains is demonstrated through composite images at each polarization; Fig. 7(a) was taken in the transmissive direction, while Fig. 7(b) was taken in the epi-direction. Note that both panels are composites of two images acquired simultaneously, and thus each panel is a polarization dMPLSM image.

The usefulness of polarization-sensitive dMPLSM for quantitative biological applications is demonstrated in Fig. 8. Here, images of fixed murine cranial nerve are imaged in TPEF and SHG simultaneously. Fluorescence in these images is due to green fluorescent protein (GFP) that is expressed in the cytoplasm of the cell; owing to the random orientation of the dipole moment of each fluorophore, the fluorescence is nominally polarization independent. The SHG response, however, is strongly dependent on the amount of coupling between the incident laser polarization and fiber orientation, particularly, as these fibers are myelinated. Thus, when activated with two differing polarizations, different structures within the sample can be visualized [see Fig. 8(d)].

C. Excitation Wavelengths

To fully observe the behavior of complex biological systems, multiple fluorophores can be introduced, each tagging to a different feature of interest within a cell. The different fluorophores often have widely varying cross sections centered at a given wavelength, and thus may not be efficiently excited by a center frequency of the femtosecond oscillator. One option is to direct multiple lasers into the microscope, using dichroics to select which wavelength to image with at a given time [46]. The difficulty of precisely matching laser repetition rates, except for identical oscillators that are designed to be locked,

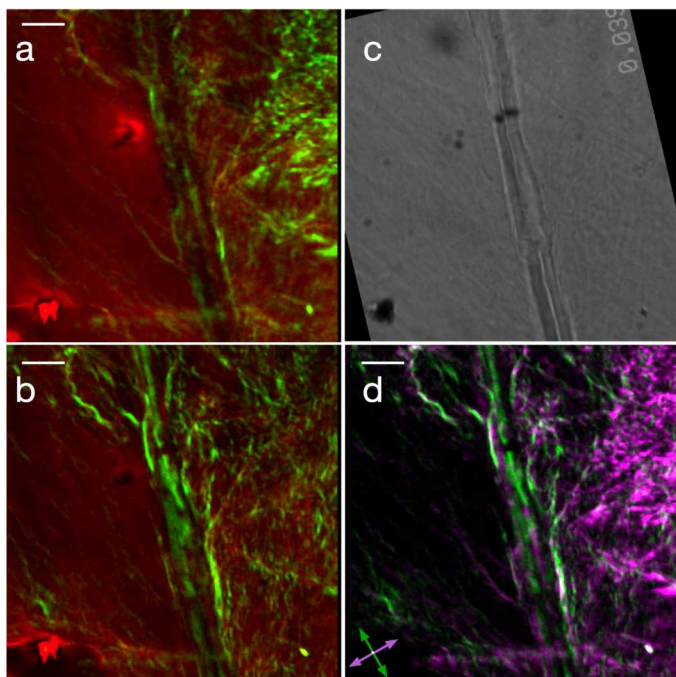


Fig. 8. Polarization dMPLSM of the trigeminal nerve from murine brain tissue, with SHG measured in transmission and fluorescence from GFP collected in the epi-direction. Panels (a) and (b) contain composite fluorescence (red) and SHG (green) images for orthogonal polarization states, while (c) contains a bright-field image of the sample. Panel (d) represents the dMPLSM image for SHG, showing a composite of the SHG response from each polarization state. The false color intensity applied to each image was chosen such that when the response from each polarization was the same, the resulting color is white. All four images comprising this figure were taken in a single scan with a Ti:Al₂O₃ oscillator, focused by a 0.75 NA/40x objective (Olympus, UPlanFL). Scale bars are 10 μm .

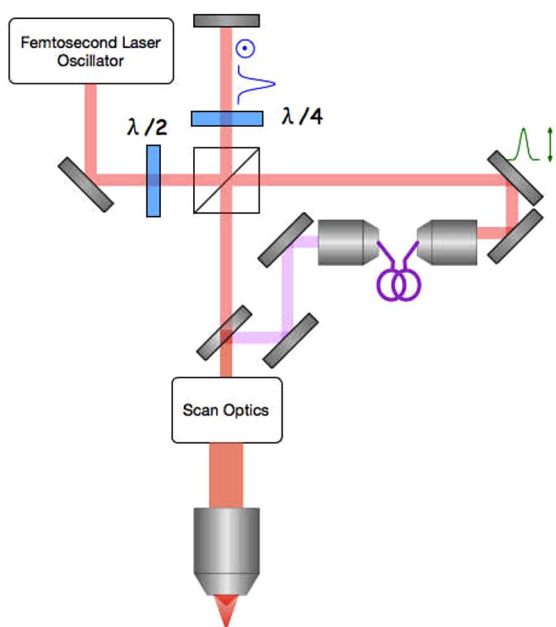


Fig. 9. Schematic of the dMPLSM system with a PCF inserted into the long arm of the interferometer. By carefully adjusting the delay of this arm, the timing is maintained to allow for electronic demultiplexing to be performed in the typical manner. Interference filters placed after the PCF allow for certain portions of the spectrum to be selected.

prevents interlacing two pulse trains for simultaneous imaging. An elegant solution is to utilize a photonic crystal fiber (PCF) to generate the bandwidth needed to activate multiple fluorophores, filtering out different portions of the resulting spectrum to be used in a two-focus dMPLSM apparatus. These fibers can generate bandwidths of 500 nm or more with modest input pulse energies (1–10 nJ) [47], [48]. They have been used in many imaging applications, including optical coherence tomography [49], [50] and coherent anti-Stokes Raman scattering spectroscopy [51]–[54]. Additionally, the output of a PCF can directly be used as a source for multiphoton imaging without postfiber compression [55]–[59].

We modified our dMPLSM system to include a PCF that was pumped by a 1040-nm femtosecond laser oscillator [see Fig. 9]. By interlacing the broadband pulse train with our 1040-nm pulse train, we enable simultaneous dual-color imaging. The 1040-nm pulse train from one arm is redirected into a 0.45-NA aspheric lens (New Focus), which focuses the pulse train into a 6-cm-long PCF [955–3.7 NL (Crystal Fibre)]. The output of the PCF is then collected with a matching aspheric lens that is on a translation stage to allow the collimation of a chosen wavelength of light. In practice, the position of the aspheric collimating lens is adjusted by placing an interference filter with the desired transmission characteristics after the lens, and then manipulating the lens until the passband of the filter is collimated. With the PCF, we are able to generate a pulsed supercontinuum with sufficient energy in wavelengths from 760–1200 nm to activate SHG.

To determine the imaging viability of the light generated from the PCF, without compression, we directed the pulse train from the PCF into our IX-71 microscope, and imaged corn starch granules, which are known to strongly generate second-harmonic light [60]. We detected SHG from 380 nm to 600 nm, with scans at selected wavelengths [see Fig. 10]. In this case, we were limited by the detector efficiency as a function of wavelength, as well as available optical filters.

Whereas the SHG images of corn starch, shown earlier (cf., Fig. 7), showed only two lobes lighting up from the linear polarization, we note that the corn starch images obtained with the PCF result in annular images from the starch. This is because the PCF does not maintain the linear input polarization; therefore, the resulting images are obtained with randomly polarized light, activating all portions of the corn starch except the central portion of the grain in which the harmoniphores are centrosymmetric.

D. Spatial Profile

A means to achieve resolution enhancement, albeit not super-resolution [61]–[65], is spatial filtering of the excitation beam by annular pupils [66]–[68]. Annular pupil filters have been used in confocal microscopy to enhance the lateral spatial resolution. Essentially, the annular filter can be viewed as a high-pass filter, as only the highest spatial frequency components are allowed to pass the objective lens. Consequently, the lateral resolution is enhanced. Since spatial resolution in MPLSM is determined only by the spatial extent of the excitation PSF, this simple method may be used to gain lateral resolution in any nonlinear contrast

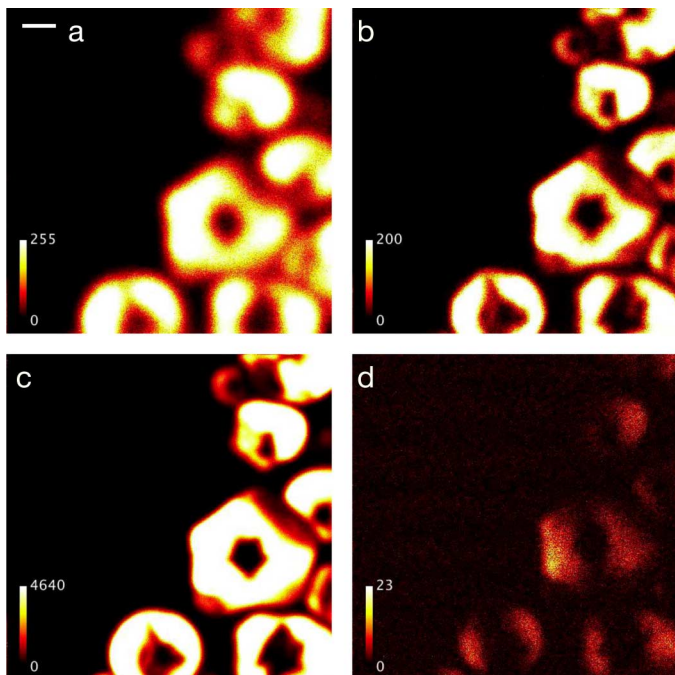


Fig. 10. Set of SHG images of corn starch taken with various portions of the PCF spectrum. SHG was detected at (a) 380 nm, (b) 450 nm, (c) 520 nm, and (d) 600 nm. All images are 512×512 pixels, with a pixel dwell time of $183 \mu\text{s}$. Scale bar is $10 \mu\text{m}$.

modality. An example of such improvement is shown in Fig. 11, in which crystalline cellulose fibers were sequentially imaged in epi-SHG with one arm of the dMPLSM system. Fig. 11(a) shows the fibers imaged with the beam filling the full numerical aperture (NA) of the excitation beam, while Fig. 11(b) shows the result when an annular pupil filter is applied. Clearly, there is an improvement in the lateral resolution of the resulting images.

Improvement in lateral resolution, however, comes at the cost of axial resolution. The axial component of the PSF is dramatically increased in annular aperture focusing because fewer k -vectors are included in the focusing cone, resulting in less cancellation of out-of-focus components. One can imagine the limiting case in which only two k -vectors are focused at $\text{NA} = 1$ in air, corresponding to a semiaperture angle of 90° . In such a case, the PSF is defined by the interference of two counterpropagating plane waves, causing the axial extent of the PSF to extend to infinity. This decrease in axial resolution is not an issue in confocal microscopy, as the confocal pinhole in the detection arm samples only a small region near the focus. However, in the whole-field detection inherent in MPLSM, the axial resolution is severely degraded. Often this is advertised as increased depth of focus, since one can detect features from a large 3-D volume, but for most applications of biological microscopy, it is imperative that the axial resolution be maintained.

The dual beams in the interferometric setup [see Fig. 1(a)] are spatially separated; therefore, it is possible to modify the spatial profile of one beam while leaving the other unaffected, similar to the axial scanning method already presented (see Fig. 4). However, instead of modifying the divergence of only one beam by image relaying the focal spot, we propose applying

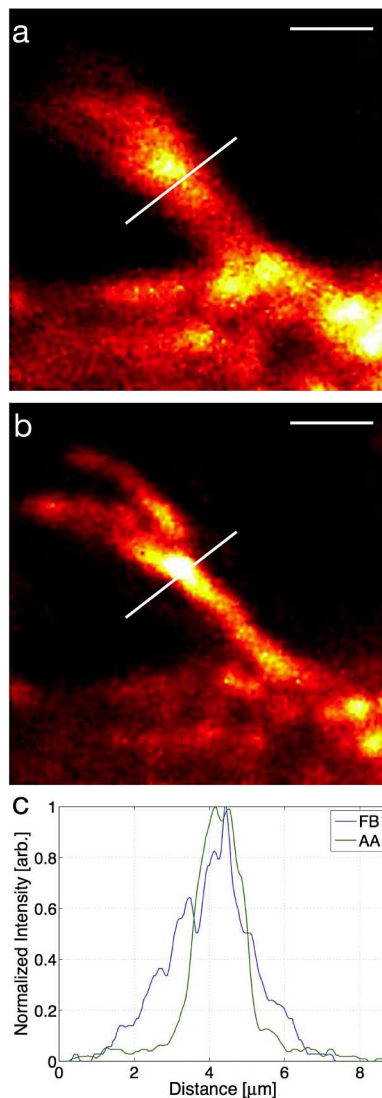


Fig. 11. Lateral resolution enhancement in SHG images of crystalline cellulose fibers. Images taken with (a) full-beam (FB) and (b) annular aperture (AA) excitation. Normalized plots of the intensity at the lineouts are shown in (c), where it is easy to see that the resolution has been greatly enhanced. Scale bars are $5 \mu\text{m}$.

an annular pupil filter to one beam, while leaving the other beam unaffected. Thus, a 3-D dataset may be acquired with enhanced lateral resolution offered by the annular aperture beam, while the axial sectioning capability can be maintained by the full-aperture beam. The simultaneous imaging capability offered by the dMPLSM system would allow one to obtain both datasets simultaneously, making it possible to perform a deconvolution of the data to obtain a single high-resolution 3-D dataset.

V. BEYOND TWO FOCI

So far, all of the dMPLSM results we have demonstrated were obtained by two foci in the specimen plane. One of the great advantages of the dMPLSM concept presented earlier, i.e., optical multiplexing and electronic demultiplexing, is the

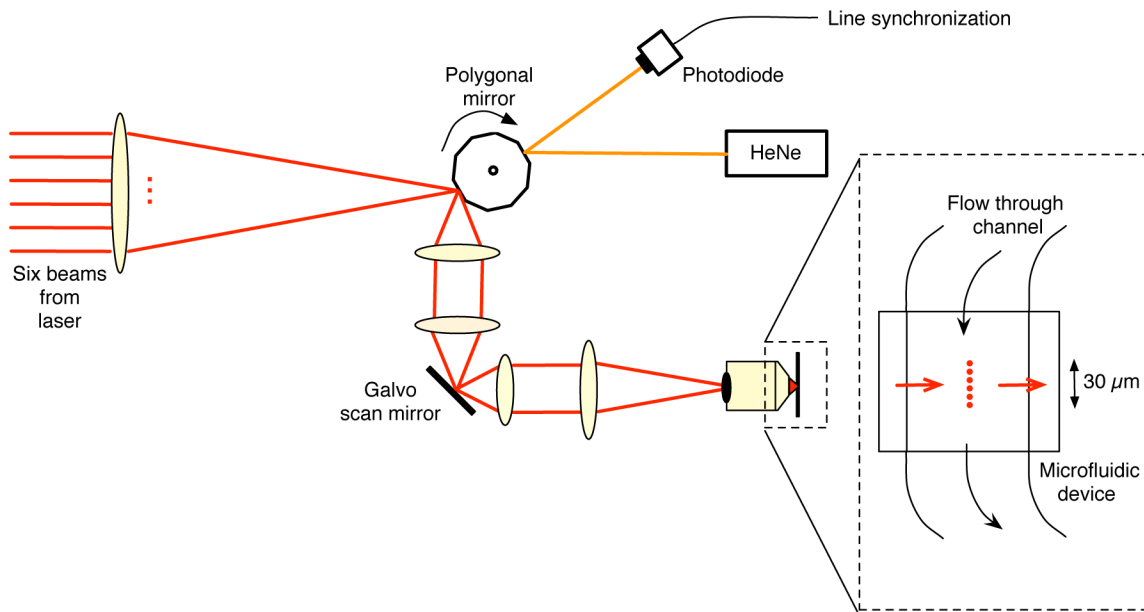


Fig. 12. Configuration of six-foci dMPLSM system using a polygonal scan mirror for imaging the flow in a microfluidic channel. The red arrows in the inset indicate scan direction of the beam array, which corresponds to left-to-right scanning in the images displayed in Fig. 13.

ability to extend the concept beyond two foci. In principle, the shortest duration that may be generated between two pulses in the LC is ~ 2 ns. As long as the temporal separation between adjacent pulses in the pulse train is at or above this threshold, electronic demultiplexing with the FPGAs is attainable. This sets an upper limit on the number of foci that may be used with a single FPGA, but it is feasible that multiple FPGAs be used to extend the capabilities of this method to any number of foci desired.

A. Six-Foci $\text{Yb:KGd}(\text{WO}_4)_2$ System

To demonstrate the use of more than two foci, we constructed a unique $\text{Yb:KGd}(\text{WO}_4)_2$ oscillator that outputs 6-fs laser beams, each appropriately time-delayed, from a single extended cavity [19]. The net output of the laser is six spatially and temporally separated beams. Temporal offset is generated purely by the round-trip time in the cavity, since each pulse is outputted from the cavity as it bounces off of the output coupler. Thus, the pulse train that is output from the cavity is a burst of six pulses, each separated by 6 ns, occurring at a repetition rate of 18.6 MHz. The pulses are 250 fs in duration and contain 19 nJ of energy per pulse.

The principle of our dMPLSM system as described in Section III is directly extended to this novel laser; only now the FPGA is programmed to contain six counters instead of two. In this system, each scan of the galvometric scan mirrors results in *six* simultaneously acquired images. Again, we can use multimodal detection to achieve 12 or 18 images per scan for bi- and trimodal detection, respectively.

Multimodal imaging with the six-beam $\text{Yb:KGd}(\text{WO}_4)_2$ system was demonstrated in [19], where 12 images of the trigeminal

nerve in murine neocortical tissue were obtained in a single scan of the galvometric mirrors.

B. Video-Rate Imaging

One clear advantage of the six-foci system is the ability to acquire images at least six times faster than a traditional MPLSM system without increasing the scan speed. The $\text{Yb:KGd}(\text{WO}_4)_2$ system presented here has the ability to image at well above video rates by acquiring multiple images per scan. We thus replaced one of the galvometric mirrors in our six-beam system with a rotating polygonal mirror to image at video rates for each focus in the system (see Fig. 12). We imaged nonfluorescent polystyrene beads flowing in a microfluidic channel in a solution of Rhodamine 6G dye. Since the foci in the six-beam system are arranged in a linear pattern within the sample, we arranged the system such that the linear array was parallel to the direction of flow in the specimen, and oriented the polygonal mirror such that we scanned the array of foci perpendicular to the direction of flow. By scanning the polygonal mirror as the beads flowed in the channel, we were able to obtain six simultaneous images of the channel (see Fig. 13). Since the foci are separated in the direction of flow, each image has the spatial coordinate along the horizontal axis, while the vertical axis represents time. We scanned the sample and acquired data at 30 Hz, resulting in pixel dwell times of $0.9 \mu\text{s}$. Note that this rate is for each of the six foci such that the true acquisition rate of the electronics is 180 Hz. With this method, we were able to determine the flow rate of the beads in the microfluidic channel to be approximately $2.5 \mu\text{m}/\text{ms}$.

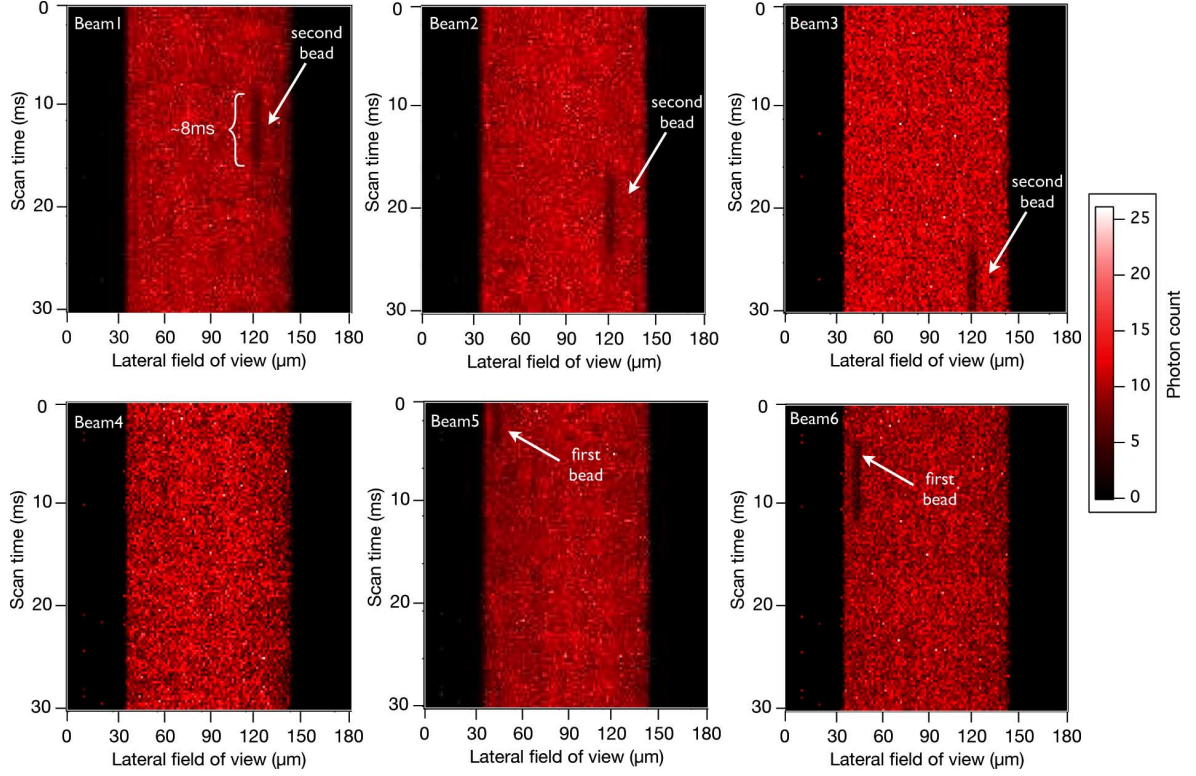


Fig. 13. Simultaneous images of nonfluorescent polystyrene beads and Rhodamine 6G flowing in a microfluidic channel. Note that the vertical axis of each image represents time, since each focus only scans in the horizontal direction.

VI. CONCLUSION

We have presented a simple scheme for simultaneous image acquisition in multiphoton microscopy with whole-field detection by a single-element detector based on optical multiplexing and electronic demultiplexing. The simultaneous imaging capability allows us to perform differential multiphoton microscopy measurements in a single shot for the first time, an advantage for *in vivo* dMPLSM assays in dynamic samples. Moreover, the spatially separated beam paths in our optical multiplexing scheme allow for various parameters to be varied independent of the other beam(s). This has allowed us to perform simultaneous imaging with two pulses of varying spectral content for the first time. Due to the widely varied two-photon absorption spectra of fluorophores and fluorescent proteins commonly used in MPLSM, the ability to vary the central wavelength of one excitation pulse with respect to the other allows for a wide array of fluorophores to be used with the same excitation source.

The orthogonal polarization states of each beam in the two-foci dMPLSM system also make it possible to perform polarization dMPLSM simultaneously for the first time. By performing polarization dMPLSM in this manner, it is possible to visualize not only the structure under study, but also to infer the phase-matching conditions within the specimen. Furthermore, exciting fluorescent specimens with orthogonal linearly polarized beams should make it possible to perform anisotropy measurements in a single shot as well, thereby extending the polarization capabilities of the system.

We have also demonstrated simultaneous dMPLSM beyond two foci with a novel six-beam Yb:KGd(WO₄)₂ oscillator, and

showed that this system is capable of video-rate imaging. Another advantage of this system is the possibility of performing stereo imaging with this microscope. Since the six foci are laterally offset from one another, it should be possible to obtain up to three stereographic images in a single shot by proper orientation of the foci in the specimen plane.

APPENDIX

CALCULATING TPE VOLUME AND PEAK INTENSITY IN FOCUS

The full vectorial calculation for the PSF near the focus of a lens has been rigorously derived by Richards and Wolf [69]. According to Zipfel *et al.* [43], fitting a Gaussian to the TPE PSF, where the TPE PSF is the intensity PSF squared, results in the following expressions for the e^{-1} point in the intensity envelope for a Gaussian spheroid:

$$\omega_{xy} = \begin{cases} \frac{0.320\lambda}{\sqrt{2NA}}, & NA \leq 0.7 \\ \frac{0.325\lambda}{\sqrt{2NA^{0.91}}}, & NA > 0.7 \end{cases} \quad (1)$$

$$\omega_z = \frac{0.532\lambda}{\sqrt{2}} \left[\frac{1}{n - \sqrt{n^2 - NA^2}} \right] \quad (2)$$

where λ is the wavelength of incident light, NA is the numerical aperture of the lens, and n is the index of refraction of the surrounding medium. By integrating the TPE PSF, Zipfel *et al.* show that the volume in which TPE occurs can be approximated

as

$$V_{\text{TPE}} = \frac{\pi^{3/2}}{0.68} \omega_{xy}^2 \omega_z. \quad (3)$$

The peak power of a pulsed laser source can be calculated from the average power, pulse duration τ , repetition rate f , and shape factor g_p according to the relation

$$P_{\text{peak}} = g P_{\text{ave}} = \frac{g_p}{\tau f} P_{\text{ave}}. \quad (4)$$

The factor g is known as the second-order temporal coherence of the pulse [70], defined as

$$g = \frac{\int_{-\infty}^{\infty} dt f I^2(t)}{\left[\int_{-\infty}^{\infty} dt f I(t)\right]^2} = \frac{g_p}{\tau f} \quad (5)$$

where $I(t)$ is the intensity of the pulse. The shape factor g_p for a Gaussian pulse is 0.664, which is what we assume throughout this manuscript. Of course, the shape factor can be calculated for any pulse shape.

Since intensity is defined as power per area, the peak power of the pulse and the radius of the spot size can be used to estimate the peak intensity in the focal plane of the microscope with the expression

$$I_{\text{peak}} = \frac{P_{\text{peak}}}{A_{xy}} = \frac{P_{\text{peak}}}{\pi \omega_{xy}^2} = g P_{\text{ave}} = \frac{g_p}{\tau f \pi \omega_{xy}^2} P_{\text{ave}}. \quad (6)$$

Note that the area used in (6) indicates the area of the intensity PSF, not the TPE PSF. We use the area in the lateral dimension because this is where the intensity of the pulse is maximal. Note also that it is straightforward to convert from the area at the $1/e$ point to other points along the Gaussian intensity by multiplicative factors. If, for example, we wished to calculate the area using the FWHM of the intensity envelope, we simply multiply the radius at e^{-1} by $\sqrt{2 \ln 2}$, resulting in a factor of $(2 \ln 2)^{-1}$ in front of the preceding expression.

ACKNOWLEDGMENT

The authors would like to thank D. N. Vitek for assistance with microfluidic devices. The distinction ‘‘differential multiphoton microscopy’’ is courtesy of Prof. V. Barzda, University of Toronto Mississauga.

REFERENCES

- [1] W. Denk, J. Strickler, and W. W. Webb, ‘‘Two-photon laser scanning fluorescence microscopy,’’ *Science*, vol. 248, pp. 73–78, 1990.
- [2] F. Helmchen and W. Denk, ‘‘Deep tissue two-photon microscopy,’’ *Nat. Methods*, vol. 2, no. 12, pp. 932–940, Dec. 2005.
- [3] D. Fu, T. E. Matthews, T. Ye, I. R. Piletic, and W. S. Warren, ‘‘Label-free *in vivo* optical imaging of microvasculature and oxygenation level,’’ *J. Biomed. Opt.*, vol. 13, pp. 040 503–1–040 503–3, 2008..
- [4] R. Hellwarth and P. Christensen, ‘‘Nonlinear optical microscopic examination of structure in polycrystalline ZnSe,’’ *Opt. Comm.*, vol. 12, pp. 318–322, 1974.
- [5] C. J. R. Sheppard, R. Kompfner, J. Gannaway, and D. Walsh, ‘‘Scanning harmonic optical microscope,’’ *IEEE J. Quantum Electron.*, vol. QE-13E, no. 9, p. 100D, Sep. 1977.
- [6] Y. Barad, H. Eisenberg, M. Horowitz, and Y. Silberberg, ‘‘Nonlinear scanning laser microscopy by third harmonic generation,’’ *App. Phys. Lett.*, vol. 70, pp. 922–924, 1997.
- [7] J. A. Squier, M. Müller, G. J. Brakenhoff, and K. R. Wilson, ‘‘Third harmonic generation microscopy,’’ *Opt. Exp.*, vol. 3, pp. 315–324, 1998.
- [8] M. D. Duncan, J. Reintjes, and T. J. Manuccia, ‘‘Scanning coherent anti-Stokes Raman microscope,’’ *Opt. Lett.*, vol. 7, pp. 350–352, 1982.
- [9] A. Zumbusch, G. R. Holtom, and X. S. Xie, ‘‘Three-dimensional vibrational imaging by coherent anti-Stokes Raman scattering,’’ *Phys. Rev. Lett.*, vol. 82, pp. 4142–4145, 1999.
- [10] J. Bewersdorf, R. Pick, and S. W. Hell, ‘‘Multifocal multiphoton microscopy,’’ *Opt. Lett.*, vol. 23, pp. 655–657, Jan. 1998.
- [11] A. H. Buist, M. Müller, J. Squier, and G. J. Brakenhoff, ‘‘Real time two-photon absorption microscopy using multi point excitation,’’ *J. Microscopy*, vol. 192, pp. 217–226, Nov. 1998.
- [12] F. Helmchen and W. Denk, ‘‘New developments in multiphoton microscopy,’’ *Curr. Opin. Neurobiol.*, vol. 12, pp. 593–601, 2002.
- [13] P. S. Tsai, J. P. Kaufhold, P. Blinder, B. Friedman, P. J. Drew, H. J. Karten, P. D. Lyden, and D. Kleinfeld, ‘‘Correlations of neuronal and microvascular densities in murine cortex revealed by direct counting and colocalization of nuclei and vessels,’’ *J. Neurosci.*, vol. 29, no. 46, pp. 14 553–14 570, Nov. 2009.
- [14] R. Carriles, K. E. Sheetz, E. E. Hoover, J. A. Squier, and V. Barzda, ‘‘Simultaneous multifocal, multiphoton, photon counting microscopy,’’ *Opt. Exp.*, vol. 16, no. 14, pp. 10 364–10 371, Jan. 2008.
- [15] J. Bewersdorf, A. Egner, and S. W. Hell, *Handbook of Biological Confocal Microscopy*, 3rd ed. New York: Springer-Verlag, Nov. 2006, ch. 29, pp. 550–560.
- [16] K. Bahlmann, P. T. C. So, M. Kirber, R. Reich, B. Kosicki, W. McGonagle, and K. Bellve, ‘‘Multifocal multiphoton microscopy (MMM) at a frame rate beyond 600 Hz,’’ *Opt. Exp.*, vol. 15, no. 17, pp. 10 991–10 998, Jan. 2007.
- [17] D. Fittinghoff, P. Wiseman, and J. Squier, ‘‘Widefield multiphoton and temporally decorrelated multifocal multiphoton microscopy,’’ *Opt. Exp.*, vol. 7, no. 8, pp. 273–279, Jan. 2000.
- [18] W. Amir, T. Planchon, C. Durfee, and J. Squier, ‘‘Simultaneous visualization of spatial and chromatic aberrations by two-dimensional Fourier transform spectral interferometry,’’ *Opt. Lett.*, vol. 31, pp. 2927–2929, Jan. 2006.
- [19] K. Sheetz, E. Hoover, R. Carriles, and D. Kleinfeld, ‘‘Advancing multifocal nonlinear microscopy: Development and application of a novel multibeam Yb:KGd(WO₄)₂ oscillator,’’ *Opt. Exp.*, vol. 16, pp. 17 574–17 584, Jan. 2008.
- [20] E. Chandler, E. Hoover, J. Field, and K. Sheetz, ‘‘High-resolution mosaic imaging with multifocal, multiphoton photon-counting microscopy,’’ *App. Opt.*, vol. 48, pp. 2067–2077, Jan. 2009.
- [21] D. Oron and Y. Silberberg, ‘‘Third-harmonic generation with cylindrical Gaussian beams,’’ *J. Opt. Soc. Amer. B*, vol. 21, pp. 1964–1968, Jan. 2004.
- [22] G. J. Brakenhoff, J. Squier, T. Norris, A. C. Bliton, M. H. Wade, and B. Athey, ‘‘Real-time two-photon confocal microscopy using a femtosecond, amplified Ti:sapphire system,’’ *J. Microsc.*, vol. 181, pp. 253–259, Jul. 1996.
- [23] D. Oron, E. Tal, and Y. Silberberg, ‘‘Scanningless depth-resolved microscopy,’’ *Opt. Exp.*, vol. 13, no. 5, pp. 1468–1476, Jan. 2005.
- [24] E. Tal, D. Oron, and Y. Silberberg, ‘‘Improved depth resolution in video-rate line-scanning multiphoton microscopy using temporal focusing,’’ *Opt. Lett.*, vol. 30, no. 13, pp. 1686–1688, 2005.
- [25] V. Andresen, A. Egner, and S. Hell, ‘‘Time-multiplexed multifocal multiphoton microscope,’’ *Opt. Lett.*, vol. 26, no. 2, pp. 75–77, 2001.
- [26] D. Fittinghoff and J. Squier, ‘‘Time-decorrelated multifocal array for multiphoton microscopy and micromachining,’’ *Opt. Lett.*, vol. 25, no. 16, pp. 1213–1215, Jan. 2000.
- [27] D. Fittinghoff, C. Schaffer, E. Mazur, and J. Squier, ‘‘Time-decorrelated multifocal micromachining and trapping,’’ *IEEE J. Sel. Top. Quantum Electron.*, vol. 7, no. 4, pp. 559–566, Jan. 2001.
- [28] M. Fricke and T. Nielsen, ‘‘Two-dimensional imaging without scanning by multifocal multiphoton microscopy,’’ *App. Opt.*, vol. 44, no. 15, pp. 2984–2988, Jan. 2005.
- [29] L. Sacconi, E. Froner, R. Antolini, M. Taghizadeh, A. Choudhury, and F. Pavone, ‘‘Multiphoton multifocal microscopy exploiting a diffractive optical element,’’ *Opt. Lett.*, vol. 28, no. 20, pp. 1918–1920, Jan. 2003.
- [30] J. Jureller, H. Kim, and N. Scherer, ‘‘Stochastic scanning multiphoton multifocal microscopy,’’ *Opt. Exp.*, vol. 14, no. 8, pp. 3406–3414, 2006.

- [31] C. B. Schaffer, B. Friedman, N. Nishimura, L. F. Schroeder, P. S. Tsai, F. F. Ebner, P. D. Lyden, and D. Kleinfeld, "Two-photon imaging of cortical surface microvessels reveals a robust redistribution in blood flow after vascular occlusion," *PLoS Biol.*, vol. 4, no. 2, pp. 0258–0270, Jan. 2006.
- [32] P. Theer, M. Hasan, and W. Denk, "Two-photon imaging to a depth of 1000 μm in living brains by use of a $\text{Ti:Al}_2\text{O}_3$ regenerative amplifier," *Opt. Lett.*, vol. 28, pp. 1022–1024, Jan. 2003.
- [33] D. Kobat, M. E. Durst, N. Nishimura, A. W. Wong, C. B. Schaffer, and C. Xu, "Deep tissue multiphoton microscopy using longer wavelength excitation," *Opt. Exp.*, vol. 17, no. 16, pp. 13 354–13 364, Jan. 2009.
- [34] K. Kim, C. Buehler, and P. So, "High-speed, two-photon scanning microscope," *App. Opt.*, vol. 38, no. 28, pp. 6004–6009, Jan. 1999.
- [35] C. Buehler, K. Kim, U. Greuter, N. Schlumpf, and P. So, "Single-photon counting multicolor multiphoton fluorescence microscope," *J. Fluorescence*, vol. 15, no. 1, pp. 41–51, Jan. 2005.
- [36] K. H. Kim, C. Buehler, K. Bahlmann, T. Ragan, W.-C. A. Lee, E. Nedivi, E. L. Heffer, S. Fantini, and P. T. C. So, "Multifocal multiphoton microscopy based on multianode photomultiplier tubes," *Opt. Exp.*, vol. 15, no. 18, pp. 11 658–11 678, Jan. 2007.
- [37] M. Kobayashi, K. Fujita, T. Kaneko, T. Takamatsu, O. Nakamura, and S. Kawata, "Second-harmonic-generation microscope with a microlens array scanner," *Opt. Lett.*, vol. 27, pp. 1324–1326, Jul. 2002.
- [38] E. J. Botcherby, M. J. Booth, R. Juškaitis, and T. Wilson, "Real-time extended depth of field microscopy," *Opt. Exp.*, vol. 16, pp. 21 843–21 848, 2008.
- [39] P. S. Tsai and D. Kleinfeld, "In vivo two-photon laser scanning microscopy with concurrent plasma-mediated ablation: Principles and hardware realization," in *Methods for In Vivo Optical Imaging*, 2nd ed., Boca Raton, FL: CRC Press, 2009, ch. 3, pp. 59–115.
- [40] A. Cheng, J. T. Gonçalves, P. Golshani, K. Arisaka, and C. Portera-Cailliau, "Spatio-temporal excitation-emission multiplexing for high-speed deep tissue in vivo 2-photon calcium imaging," no. 484.5. Society for Neuroscience, 2009.
- [41] Two-photon action cross sections. [Online]. Available: <http://www.drbio.cornell.edu/TextDataFiles/YFP.txt>.
- [42] R. W. Boyd, *Nonlinear Optics*, 2nd ed. New York: Academic, 2003.
- [43] W. R. Zipfel, R. M. Williams, and W. W. Webb, "Nonlinear magic: multiphoton microscopy in the biosciences," *Nat. Biotechnol.*, vol. 21, no. 11, pp. 1369–1377, Nov. 2003.
- [44] R. Brown, A. Millard, and P. Campagnola, "Macromolecular structure of cellulose studied by second-harmonic generation imaging microscopy," *Opt. Lett.*, vol. 28, pp. 2207–2209, Jan. 2003.
- [45] O. Nadiarykh, R. LaComb, P. Campagnola, and W. Mohler, "Coherent and incoherent SHG in fibrillar cellulose matrices," *Opt. Exp.*, vol. 15, pp. 3348–3360, Jan. 2007.
- [46] R. Carriles, D. N. Schafer, K. E. Sheetz, J. J. Field, R. Cisek, V. Barzda, A. W. Sylvester, and J. A. Squier, "Invited review article: Imaging techniques for harmonic and multiphoton absorption fluorescence microscopy," *Rev. Sci. Instrum.*, vol. 80, pp. 081 101–1–081 101–23, 2009.
- [47] J. K. Ranka, R. S. Windeler, and A. J. Stentz, "Visible continuum generation in air-silica microstructure optical fibers with anomalous dispersion at 800 nm," *Opt. Lett.*, vol. 25, pp. 25–27, 2000.
- [48] W. J. Wadsworth, A. Ortigosa-Blanch, J. C. Knight, T. A. Birks, T.-P. M. Man, and P. S. J. Russell, "Supercontinuum generation in photonic crystal fibers and optical fiber tapers: A novel light source," *J. Opt. Soc. Amer. B*, vol. 19, pp. 2148–2155, 2002.
- [49] S. Bourquin, A. D. Aguirre, I. Hartl, P. Hsiung, T. H. Ko, and J. G. Fujimoto, "Ultrahigh resolution real time OCT imaging using a compact femtosecond Nd:Glass laser and nonlinear fiber," *Opt. Exp.*, vol. 11, pp. 3290–3297, 2003.
- [50] G. Humbert, W. J. Wadsworth, S. G. Leon-Saval, J. C. Knight, T. A. Birks, and P. S. J. Russell, "Supercontinuum generation system for optical coherence tomography based on tapered photonic crystal fibre," *Opt. Exp.*, vol. 14, pp. 1596–1603, 2006.
- [51] E. R. Andresen, H. N. Paulsen, V. Birkedal, J. Thogersen, and R. K. Soren, "Broadband multiplex coherent anti-Stokes Raman scattering microscopy employing photonic-crystal fibers," *J. Opt. Soc. Amer. B*, vol. 22, pp. 1934–1938, 2005.
- [52] H. Wang, T. B. Huff, and J.-X. Cheng, "Coherent anti-Stokes Raman scattering imaging with a laser source delivered by a photonic crystal fiber," *Opt. Lett.*, vol. 31, pp. 1417–1419, 2006.
- [53] E. R. Andresen, C. K. Nielsen, J. Thogersen, and S. R. Keiding, "Fiber laser-based light source for coherent anti-Stokes Raman scattering microspectroscopy," *Opt. Exp.*, vol. 15, pp. 4848–4856, 2007.
- [54] M. Okuno, H. Kano, P. Leproux, V. Couderc, and H. o Hamaguchi, "Ultrabroadband multiplex CARS microspectroscopy and imaging using a subnanosecond supercontinuum light source in the deep near infrared," *Opt. Lett.*, vol. 33, pp. 923–925, 2008.
- [55] L. Fu and M. Gu, "Double-clad photonic crystal fiber coupler for compact nonlinear optical microscopy imaging," *Opt. Lett.*, vol. 31, pp. 1471–1473, 2006.
- [56] K. Isobe, W. Watanabe, S. Matsunaga, T. Higashi, K. Fukui, and K. Itoh, "Multi-spectral two-photon excited fluorescence microscopy using supercontinuum light source," *Jap. J. Appl. Phys.*, vol. 44, pp. L167–L169, 2005.
- [57] G. McConnell, "Confocal laser scanning fluorescence microscopy with a visible continuum source," *Opt. Exp.*, vol. 12, pp. 2844–2850, 2004.
- [58] J. A. Palero, V. O. Boer, J. C. Vijverberg, H. Gerritsen, and H. J. C. M. Sterenborg, "Short-wavelength two-photon excitation fluorescence microscopy of tryptophan with a photonic crystal fiber based light source," *Opt. Exp.*, vol. 13, pp. 5363–5368, 2005.
- [59] J. R. Unruh, E. S. Price, R. G. Molla, L. Stehno-Bittel, C. K. Johnson, and R. Hui, "Two-photon microscopy with wavelength switchable fiber laser excitation," *Opt. Exp.*, vol. 14, pp. 9825–9831, 2006.
- [60] G. Mizutani, Y. Sonoda, H. Sano, M. Sakamoto, T. Takahashi, and S. Ushioda, "Detection of starch granules in a living plant by optical second harmonic microscopy," *J. Lumin.*, vol. 87–89, pp. 824–826, 2000.
- [61] S. W. Hell and J. Wichmann, "Breaking the diffraction resolution limit by stimulated emission: Stimulated-emission-depletion fluorescence microscopy," *Opt. Lett.*, vol. 19, pp. 780–782, Jan. 1994.
- [62] E. Betzig, G. H. Patterson, R. Sougrat, O. W. Lindwasser, S. Olenych, J. S. Bonifacino, M. W. Davidson, J. Lippincott-Schwartz, and H. F. Hess, "Imaging intracellular fluorescent proteins at nanometer resolution," *Science*, vol. 313, no. 5793, pp. 1642–1645, Sep. 2006.
- [63] M. J. Rust, M. Bates, and X. Zhuang, "Sub-diffraction-limit imaging by stochastic optical reconstruction microscopy (STORM)," *Nat. Methods*, vol. 3, no. 10, pp. 793–796, Oct. 2006.
- [64] S. W. Hell, "Far-field optical nanoscopy," *Science*, vol. 316, pp. 1153–1158, Jan. 2007.
- [65] O. Masihzadeh, P. Schlup, and R. A. Bartels, "Enhanced spatial resolution in third-harmonic microscopy through polarization switching," *Opt. Lett.*, vol. 34, no. 8, pp. 1240–1242, Jan. 2009.
- [66] S. W. Hell, "Improvement of lateral resolution in far-field fluorescence light microscopy by using two-photon excitation with offset beams," *Opt. Comm.*, vol. 106, pp. 19–24, 1994.
- [67] M. Martínez-Corral, P. Andrés, C. J. Zapata-Rodríguez, and M. Kowalczyk, "Three-dimensional superresolution by annular binary filters," *Opt. Comm.*, vol. 165, pp. 267–278, 1999.
- [68] C. J. R. Sheppard and A. Choudhury, "Annular pupils, radial polarization, and superresolution," *App. Opt.*, vol. 43, pp. 4322–4327, 2004.
- [69] B. Richards and E. Wolf, "Electromagnetic diffraction in optical systems. II. Structure of the image field in an aplanatic system," *Proc. Royal Soc. London A*, vol. 253, no. 1274, pp. 358–379, 1959.
- [70] C. Xu and W. W. Webb, "Measurement of two-photon excitation cross sections of molecular fluorophores with data from 690 to 1050 nm," *J. Opt. Soc. Amer. B*, vol. 13, pp. 481–491, 1996.

Jeffrey J. Field received the B.Sc. and M.Sc. degrees in engineering physics in 2005 and 2006, respectively, and the Ph.D. degree in applied physics, in 2010, all from the Colorado School of Mines, Golden.

He is currently a Postdoctoral Fellow in the Center for Microintegrated Optics for Advanced Bioimaging and Control, Colorado School of Mines.

Dr. Field is a member of the Optical Society of America, and the Society of Photo-Optical Instrumentation Engineers.

Kraig E. Sheetz was born in Uniontown, PA, in 1968. He received the Ph.D. degree from the Colorado School of Mines, Golden, in 2009.

He is a Lieutenant Colonel in the U.S. Army and is currently an Academy Professor in the Department of Physics and Nuclear Engineering, U.S. Military Academy, West Point, NY. His research interests include ultrafast solid-state laser design and nonlinear microscopy.

Eric V. Chandler received two B.Sc. degrees in engineering physics and chemistry, in 2006, and the M.Sc. degree in applied physics, in 2007, all from the Colorado School of Mines, Golden.

He is currently a Graduate Fellow of the Renewable Energy Materials Research Science and Engineering Center, Colorado School of Mines. His research focuses on the use of nanomaterials in photovoltaics.

Mr. Chandler is a Student Member of the Optical Society of America and the American Chemical Society.

Erich E. Hoover received the B.Sc. degree in engineering physics, in 2007, and the M.Sc. degree in engineering with an electrical specialty, in 2008, from the Colorado School of Mines, Golden, where he is currently working toward the Ph.D. degree in applied physics.

He was a Computer Programmer and Software Engineer at dBm Optics, Inc. for seven years. His current research interests include applying photon counting techniques toward simultaneous imaging of multiple depths inside scattering media.

Mr. Hoover has been a member of the American Physical Society, since 2009.

Michael D. Young received the B.Sc. degree in engineering physics, in 2008, from the Colorado School of Mines, Golden, where he is currently working toward the Ph.D. degree.

His research interests include simulated optical design, laser microscopy, and physics pedagogy.

Shi You-Ding was born in Anhui, China, in 1966. He received the Ph.D. degree in plant biology from the Chinese Academy of Sciences, Beijing, China, in 1994.

He was involved in Postdoctoral training at the Weizmann Institute of Sciences, Israel conducting biochemistry research on bacterial cellulosomal systems for three years. He is currently a Senior Scientist and the Team Leader in the Biosciences Center, National Renewable Energy Laboratory (NREL), Golden, CO, and also the Project Leader in the BioEnergy Science Center (BESC), in collaboration with Oak Ridge National Laboratory (ORNL). He discovered three complex enzyme systems that could be applied to biomass conversion process. He is the author or coauthor of more than 60 publications, and holds 6 U.S. patents that have been licensed to industry in addition to having several more NREL Records of Invention in progress.

Dr. You-Ding is on the Editorial Board of *Biotechnology for Biofuels* and *BioResources*, and is a member of the American Society of Microbiology (ASM), the American Chemical Society (ACS), the Materials Research Society (MRS), the American Association for the Advancement of Science (AAAS), and the Biophysical Society.

Anne W. Sylvester, photographs and biography not available at time of publication.

David Kleinfeld received the B.S.E.E degree from the University of Illinois, Urbana-Champaign, including a stint off to apprentice at Argonne National Laboratories, IL, from where he also received the M.Sc. degree in physics. He received the Ph.D. degree in physics from the University of California, San Diego.

After completion of the Ph.D. degree, he was at AT&T Bell Laboratories, Murray Hill, NJ. Since then, he has been with the Department of Physics, University of California, San Diego. His research interests include issues in systems neuroscience, specifically active sensation and cortical blood flow. Many of these studies involve linear and non-linear optical recording techniques. He is active in postgraduate education. He was the Co-Director of the "Methods in Computational Neuroscience" and "NeuroInformatics" courses at the Marine Biological Laboratory, Woods Hole, MA, and the \mathcal{O} Imaging Structure and Function \mathcal{O} course at Cold Spring Harbor Laboratories, NY.

Jeff A. Squier received the B.Sc. degree in engineering physics, and the M.Sc. degree in applied physics from the Colorado School of Mines, Golden, and the Ph.D. degree in optics, in 1992, from the University of Rochester, Rochester, NY. His Ph.D. thesis was focused on the development of solid-state femtosecond chirped pulse amplification systems.

He was a Research Faculty at the Center for Ultrafast Optical Science, University of Michigan, and in 1995, joined the University of California, San Diego (UCSD). He was involved in the development of and application of femtosecond laser sources at UCSD until 2002. Since then, he has been with the Department of Physics, Colorado School of Mines, Golden. He has authored or coauthored more than 190 papers in international journals and conferences, and holds multiple patents.

Dr. Squier was a member of the Optical Society of America, and became a Fellow in 2000.